Environmental Science Advances

ROYAL SOCIETY OF CHEMISTRY

PAPER

View Article Online
View Journal | View Issue

Cite this: *Environ. Sci.: Adv.*, 2022, **1**, 59

Matrix effects on the performance and mechanism of Hg removal from groundwater by MoS_2 nanosheets†

Mengxia Wang,[a] Qi Han,[a] Yufei Shu,[a] Kunkun Wang,[a] Li Wang,[a] Bei Liu,[a] Ines Zucker [b] and Zhongying Wang *[a]

Mercury (Hg) contamination in groundwater has been recognized as a serious threat to human health and ecological systems all over the world. This study demonstrated that two-dimensional (2D) molybdenum disulfide (MoS_2) nanosheets can efficiently remove Hg in groundwater, with high Hg uptake capacity, ultrafast removal kinetics, and excellent selectivity. Interestingly, we found that the groundwater matrix has profound implications on the Hg removal efficiency and mechanisms by MoS_2 nanosheets. Specifically, surface adsorption is the dominant removal mechanism for Hg in DI water owing to the high affinity between Hg(II) and MoS_2 *via* strong Lewis acid/base soft–soft interactions. In groundwater, however, the presence of Cl^- renders HgClOH the dominant species, which can undergo adsorption onto MoS_2 and homolytic cleavage to form the $^{\bullet}$HgCl radical. As an intermediate radical, $^{\bullet}$HgCl could either dimerize to form Hg_2Cl_2 or further reduce to Hg^0. This reduction-based mechanism enhanced the overall removal capacity of Hg to 6288 mg g^{-1}, which is among the highest values reported to date. Additionally, our desorption tests revealed the high stability of immobilized Hg on MoS_2 nanosheets over conventional adsorbents in various extractant fluids. These impressive features render MoS_2 nanosheets a promising candidate for remediation of Hg-contaminated groundwater.

Received 22nd November 2021
Accepted 12th January 2022

DOI: 10.1039/d1va00035g

rsc.li/esadvances

Environmental significance

Mercury (Hg) contamination is a serious threat to human health and ecological systems, and requires efficient remediation methods. Two-dimensional MoS_2 has emerged as a promising material for Hg remediation. Investigation for the matrix effects on Hg removal efficiency by MoS_2 nanomaterials is imperative and a precondition for the application in various water systems (*e.g.*, groundwater). This study employed chemically exfoliated MoS_2 nanosheets to remove Hg(II) in groundwater, and demonstrated that the coexisting Cl– has largely promoted the removal performance through the reductive formation of Hg_2Cl_2. The highest capacity reported so far has further advanced the potential of utilizing MoS_2-based nanomaterials in Hg remediation and highlighted the significance of matrix effects in the nano-enabled remediation processes.

[a]*State Environmental Protection Key Laboratory of Integrated Surface Water-Groundwater Pollution Control, Guangdong Provincial Key Laboratory of Soil and Groundwater Pollution Control, School of Environmental Science and Engineering, Southern University of Science and Technology, Shenzhen 518055, China. E-mail: wangzy6@sustech.edu.cn; Tel: +86-075588018040*

[b]*Porter School of Environmental Studies, School of Mechanical Engineering, Tel Aviv University, 69978, Israel*

† Electronic supplementary information (ESI) available: Schematic illustration of the chemical exfoliation of bulk MoS_2 (Fig. S1); particle size distribution of the as-exfoliated MoS_2 nanosheets (Fig. S2); S 2p XPS spectra of the as-prepared MoS_2 nanosheets (Fig. S3); Hg uptake kinetics by MoS_2 nanosheets in groundwater (Fig. S4); Hg uptake kinetics model fitting curve (Fig. S5); determination of MoO_4^{2-} in solution by ion chromatography (Fig. S6); Ca(II) and Mg(II) uptake by MoS_2 nanosheets (Fig. S7); XPS survey scan spectra of Hg-laden MoS_2 formed in DI water and groundwater (Fig. S8); TEM images and EDS-mapping of Hg-laden MoS_2 nanosheets in groundwater (Fig. S9) and DI water (Fig. S10); mass distribution of Mo in groundwater and DI water (Fig. S11); oxidation of MoS_2 nanosheets in the presence of Cl^- at various concentrations (Fig. S12); the percentage of Hg species in simulated groundwater (Fig. S13); effects of pH on Hg removal efficiency by MoS_2 (Fig. S14); Hg uptake by AC in groundwater (Fig. S15). See DOI: 10.1039/d1va00035g

1. Introduction

Mercury (Hg) is recognized as one of the most remarkably toxic contaminants and widely present in environmental matrices such as soil and groundwater.[1,2] Generally, Hg in the environment is generated from industrial activities, agriculture, and natural sources.[3–6] In groundwater, Hg mainly exists as inorganic species (an average of 84% of soluble Hg)[7] and Hg pollution occurs *via* deep-well disposal of liquid wastes, the leachate from a number of contaminated sources such as landfills, sewage, mine tailings, and industrial waste lagoons.[8] Exposure to Hg has been reported to cause various adverse health effects on the nervous, renal, and endocrine systems.[9] Based on surrounding environmental conditions, the environmental and health risk of Hg in groundwater can be intensified by the microbial transformation of inorganic Hg to the more toxic methylmercury, which can be biomagnified with

a bioaccumulation factor of up to 10^6 in the food chain.[10] Consequently, the United States Environmental Protection Agency (EPA) has established a maximum contaminant level (MCL) of 2 μg L^{-1} for Hg, and the guideline value from the World Health Organization (WHO) is set to be 1 μg L^{-1}.[11] Nowadays, exposure to Hg-contaminated drinking water is still a serious concern in some small and rural communities, where groundwater is directly used for self-supply domestic purposes without standard treatment.

Available techniques for removing Hg from aqueous solutions include chemical precipitation,[12,13] ion exchange,[14] coagulation,[15] membrane filtration,[16] and adsorption.[17] Among these techniques, adsorption is a favored option for small-sized communities, because of feasible operation, low expertise requirement, and regeneration potential. Conventional adsorbents (*e.g.*, carbon-based materials,[18,19] iron-based minerals,[20,21]and oxide nanomaterials[11]) generally have low specificity and affinity to Hg, which leads to the low effectiveness of Hg removal. Particularly in the case of Hg removal from groundwater, co-existing cations at elevated concentrations relative to Hg may compete with Hg cations for the sorption sites and therefore increase the necessary sorbent dose and costs. For instance, the typical concentrations of Ca and Mg ions in groundwater can range from ~10 to 200 mg L^{-1}, a few orders of magnitude higher than that of the Hg species found in contaminated groundwater.[22,23] Additionally, the presence of various anions (*e.g.*, Cl^-, NO_3^-, OH^-, and SO_4^{2-})[24,25] and negatively-charged natural organic matter (NOM) may form various stable coordination complexes with Hg(II), which may reduce the overall removal efficiency of Hg from groundwater.

Two dimensional molybdenum disulfide (2D-MoS_2), an emerging nanomaterial, consists of covalently bonded atomic trilayers of S–Mo–S and has been extensively studied with demonstrated excellent removal performance towards various heavy metals including Hg.[26–28] Generally, the highly efficient and selective Hg removal by MoS_2 nanosheets stems from their large surface area and abundant active sulfur sites that have strong Lewis acid/base soft–soft interactions with Hg.[29–31] Liu *et al.*[32] used hydrothermally-synthesized MoS_2 to simultaneously remove Hg(II), Pb(II) and Cd(II) from the aqueous phase, and MoS_2 exhibited the highest removal efficiency for Hg(II) among the tested ions with a maximum adsorption capacity of 2409 mg g^{-1}. Jia *et al.*[33] reported multi-layer adsorption of Hg(II) onto MoS_2 nanosheets *via* Hg–S complexation and electrostatic interactions. Additionally, MoS_2-based complex architectures have been developed for enhanced exposure of the sorption sites and feasible regeneration of the sorbent materials. For instance, MoS_2 nanoflowers were immobilized onto eco-friendly aerogels and exhibited excellent removal efficiency of methylmercury and also extremely low toxicity to aquatic species.[34–36] MoS_2-loaded carbon nanofibers were employed to maximize the exposure of MoS_2 surface to Hg for enhanced decontamination while minimizing the release of loaded MoS_2 into the treated water.[37] Despite superb Hg removal performance by MoS_2, previous studies mainly focused on Hg removal in deionized (DI) water or buffered solutions.[32,37–39] Considering limited pretreatment approaches for rural communities to moderate the impacts of groundwater constituents, we believe it is of great importance to study the matrix effects on the Hg removal from groundwater, and to unravel the applicability of MoS_2 in the remediation of Hg-contaminated groundwater.

The overall goal of this work was to determine the mechanisms governing removal of Hg(II) from groundwater by 2D MoS_2 nanosheets and examine the effects of the groundwater matrix on the Hg(II) removal efficacy. In this work, monolayer MoS_2 nanosheets were prepared by a chemical exfoliation method and employed for evaluating the Hg(II) removal performance of MoS_2 nanosheets in groundwater. The Hg removal kinetics and isotherms of MoS_2 were studied in batch tests and compared in groundwater and DI water to reveal any matrix effects. The Hg-laden MoS_2 formed in groundwater and DI was extensively characterized to understand the underlying Hg removal mechanisms in each water matrix. Lastly, the stability of Hg immobilized by MoS_2 nanosheets was tested in various extractant solutions to test the Hg anchoring capability in groundwater remediation.

2. Materials and methods

2.1 Preparation and characterization of MoS_2 nanosheets

The detailed information of chemicals used in this study is listed in the ESI.† MoS_2 nanosheets were prepared by an established chemical exfoliation method following the approach reported previously, and the schematic illustration of the exfoliation process is shown in Fig. S1.†[40] Briefly, 5 mL of 1.6 M *n*-butyllithium in hexane solution was added to ~300 mg of bulk MoS_2 powder (~2 μm, Sigma-Aldrich) and the suspension was stirred gently in a nitrogen-filled glovebox for 2 d. Then 40 mL hexane was added to the resulting solution mixture, and the excess organic reactants and byproducts were removed by centrifugation at 4000 rpm for 15 min to obtain the Li-intercalated MoS_2 sample. About 100 mL DI water was added to the collected Li-intercalated MoS_2 and incubated in an ultrasonic water bath for 1 h to facilitate hydration and exfoliation to obtain individual MoS_2 nanosheets. The resulting dispersion of MoS_2 nanosheets was dialyzed in DI water for 1 d using a dialysis bag (BEF 88244, Thermo Fisher Scientific, Waltham, MA, U.S.A.) to remove inorganic byproduct LiOH. Finally, the MoS_2 stock solution was purged with purified N_2 (>99.9%) for 1 h to remove dissolved oxygen and stored in a nitrogen-filled glovebox. To determine the nanosheet concentration, the MoS_2 suspension was completely digested with 2% HNO_3 and 30% H_2O_2, followed by the measurement of soluble Mo species concentration with ICP-OES (iCAP 7000 SERIES, Thermo Fisher Scientific, Waltham, MA, U.S.A.).

The hydrodynamic size and zeta potential (ζ) of MoS_2 nanosheets were obtained using a Zetasizer Nano ZS instrument (NanoBrook Omini, Brookhaven, NY, U.S.A.). An atomic force microscope (AFM, MFP-3D Stand Alone, Asylum Research, Oxford, UK) was used to observe the flake-like structure of MoS_2 nanosheets. Transmission electron microscopy (TEM, Talos F200X, FEI, MA, U.S.A.) with energy dispersive spectroscopy (EDS) was used to monitor the morphology of the as-exfoliated MoS_2 and exhibit the elemental distribution of Hg-laden MoS_2

nanosheets. Raman spectroscopic measurements were performed on a LabRAM HR Evolution (HORIBA, Kyoto, Japan). X-ray photoelectron spectroscopy (XPS, PHI 5000 Versaprobe III, ULVAC-PHI, Japan) was employed to identify the chemical composition of the MoS_2 nanosheets before and after Hg removal. The composition and crystallographic structure of Hg-laden MoS_2 nanosheets were examined by powder X-ray diffraction (XRD, Rigaku Smartlab 9 kW, Tokyo, Japan) with Cu-Kα radiation ($\gamma = 1.5406$ Å).

2.2 Mercury removal by MoS_2 nanosheets

Batch tests were used to study the Hg(II) removal capacity, kinetics, and selectivity of MoS_2 nanosheets in groundwater. A solution of pH 8.3 containing 230 mg L^{-1} Na^+, 32 mg L^{-1} Ca^{2+}, 234 mg L^{-1} Cl^-, 183 mg L^{-1} HCO_3^-, and 96 mg L^{-1} SO_4^{2-} was prepared to represent the simulated groundwater.[41] To evaluate the removal kinetics, the simulated groundwater was spiked with 20 mg L^{-1} Hg, and 4 mg L^{-1} MoS_2 dispersion was then added to initiate the remediation. The mixture was continuously mixed on an end-over-end rotator at 60 rpm at room temperature (25 ± 1 °C). At predetermined time intervals (0–48 h), the samples were filtered through 0.22 μm PTFE filters and the remaining Hg concentrations in the filtrates were measured with a direct mercury analyzer (DMA-80, Milestone, Italy). The pH of the mixture was stable at 7.9 ± 0.2 throughout the entire removal process. The Hg uptake isotherm was determined with the initial concentration of MoS_2 nanosheets at 4 mg L^{-1} and varying initial Hg(II) concentrations from 2 to 42 mg L^{-1}. Upon equilibration for 2 d, the samples were processed in the same manner as described in the sorption kinetics tests. To reveal the groundwater matrix effects on Hg capture, the Hg uptake isotherm was also measured in DI water for comparison. The equilibrium Hg removal capacity (q_e, mg Hg/g MoS_2) and the distribution coefficient (K_d) were calculated *via* the following equations:

$$q_e = (C_0 - C_e)V/m \quad (1)$$

$$K_d = (V[(C_0 - C_e)/C_e])/m \quad (2)$$

where C_0 and C_e are the initial and equilibrium Hg concentrations (mg L^{-1}) after Hg removal by MoS_2, respectively, V is the solution volume (L), and m is the mass (g) of MoS_2.

In addition, to demonstrate the selectivity of MoS_2 towards Hg among various typical heavy metal cations, batch experiments were performed under the same conditions except for the addition of Ni(II), Cd(II), Cu(II), and Zn(II) at 1 mg L^{-1} as co-existing cations. All experiments were conducted in duplicate. To investigate the effects of pH on Hg immobilization, the initial pH was adjusted in the range of 3–8 with the addition of HNO_3 and NaOH solutions. In order to probe the competing ion effects on Hg removal, $Ca(NO_3)_2$ and $Mg(NO_3)_2$ were spiked in the sorption tests with Ca(II) or Mg(II) concentrations up to 200 mg L^{-1} to mimic groundwater with high hardness. The effects of NOM on the Hg removal were tested in the presence of various concentrations of NOM (0–50 mg L^{-1}).

2.3 Mechanistic investigation of groundwater matrix effects

To reveal the removal mechanisms, we investigated the mass distribution of Hg in the remaining solution (*i.e.*, unremoved Hg), with the MoS_2 sorbent (*i.e.*, Hg sorbed), and in the vapor state (*i.e.*, reduced Hg^0). First, the Hg concentration in solution at equilibrium was measured following the filtration stage as described before. The Hg-laden MoS_2 was collected on the membrane surface and freeze-dried to drive off water and Hg^0. Freeze-drying was performed under vacuum conditions at −45 °C using a vacuum freeze-dryer (Scientz-12N, Ningbo Xinzhi Biotech Co., Ltd., China) for 36 h. A solution made of 30% H_2O_2 and 68% HNO_3 was then used to completely digest the Hg-laden MoS_2 to enable quantification of the Hg (and Mo) content on the adsorbent. Finally, the amount of Hg^0 was obtained by subtracting the amount of Hg remaining in the solution and on the sorbents from the total amount of Hg added. All experiments were conducted in triplicate to ensure reproducibility.

3. Results and discussion

3.1 Characterization of MoS_2 nanosheets

The dispersion of MoS_2 nanosheets was prepared by chemical exfoliation of bulk MoS_2 reported previously (Fig. S1†).[35] After exfoliation, the lateral size of the as-prepared MoS_2 nanosheets was estimated to be ~230 nm (Fig. S2†), and the zeta potential was −44.7 mV at pH 6.0. The MoS_2 suspension was able to maintain colloidal stability (Fig. S1†) for over 6 months due to strong electrostatic repulsion forces between the negatively charged nanosheets, which is critical to allow the contact between MoS_2 and the target Hg cations. TEM and AFM images (Fig. 1a and b) exhibited the flake-like structure of exfoliated MoS_2 nanosheets, and the thickness measured by AFM implied that most nanosheets existed as monolayers or bi-layers. The phase composition of the as-exfoliated MoS_2 was characterized by XPS and Raman spectroscopy. As shown in Fig. 1c, the deconvolution of Mo 3d XPS spectra implied that 1T-MoS_2 was the dominant phase at 228.5 and 231.6 eV, corresponding to Mo $3d_{5/2}$ and Mo $3d_{3/2}$, respectively.[42] 2H phase MoS_2, as a minor component in the exfoliated nanosheets, exhibited a binding energy ~1 eV higher than that of the 1T phase. The mixed phase in the as-exfoliated MoS_2 was also confirmed with S 2p XPS spectra (Fig. S3†) and Raman spectra (Fig. 1d), which exhibited characteristic peaks of 1T (*i.e.*, 149.1, 214.2, and 323.5 cm^{-1}) and 2H phases (*i.e.*, 377.2 and 402.0 cm^{-1}).[43,44] The partial phase conversion from pure 2H in bulk MoS_2 to mixed 1T/2H in the exfoliated MoS_2 was caused by lithium intercalation in chemical exfoliation.[45]

3.2 Hg removal performance by MoS_2 nanosheets

Batch experiments were performed to examine the effectiveness of the as-prepared MoS_2 nanosheets in the removal of Hg in the groundwater matrix. As shown in Fig. 2a, MoS_2 nanosheets exhibited fast Hg(II) removal kinetics with a removal efficiency of 95% achieved within 5 min. More importantly, at a moderate MoS_2 dose of 8 mg L^{-1}, the concentration of Hg was reduced

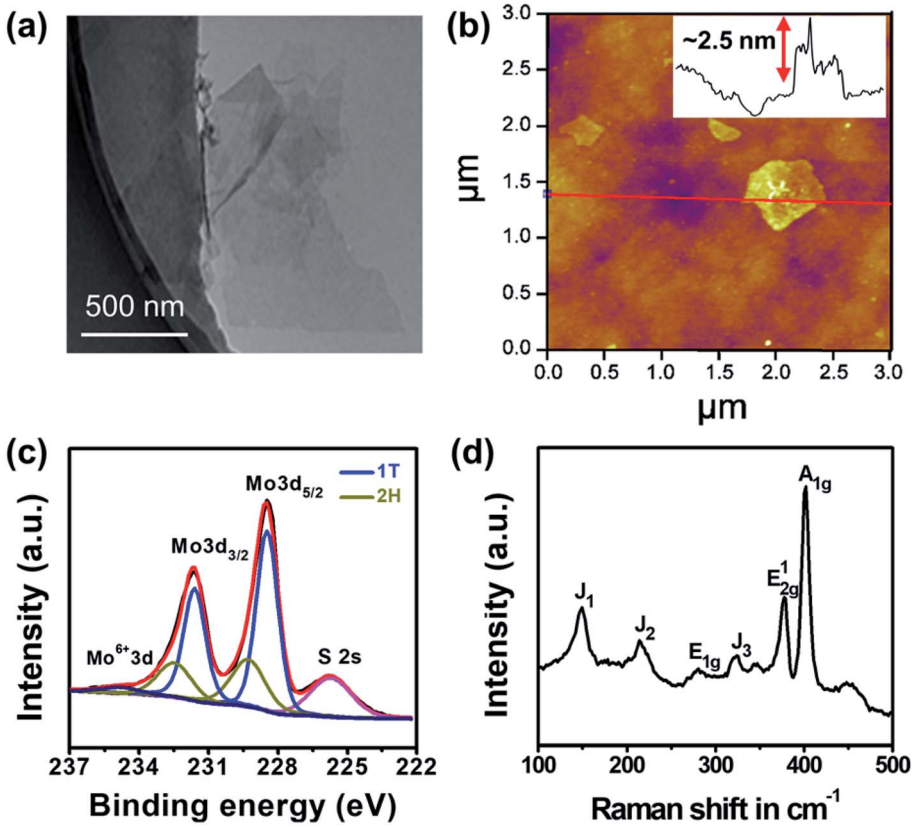

Fig. 1 Characterization of the as-exfoliated MoS_2 nanosheets. (a) TEM and (b) AFM images of MoS_2 nanosheets, and the inset shows the line profile; (c) Mo 3d XPS and (d) Raman spectra.

from 5 mg L^{-1} to 0.92 μg L^{-1} (Fig. S4†), far below the drinking water standard regulated by the US-EPA (2 μg L^{-1}). The distribution coefficient (K_d) of MoS_2 nanosheets for Hg is also calculated to be 1.02×10^8 mL g^{-1}, which is much higher than 1.0×10^5 mL g^{-1}, the criterion for excellent adsorbents.[31] This value is also superb among engineered nanomaterials targeted

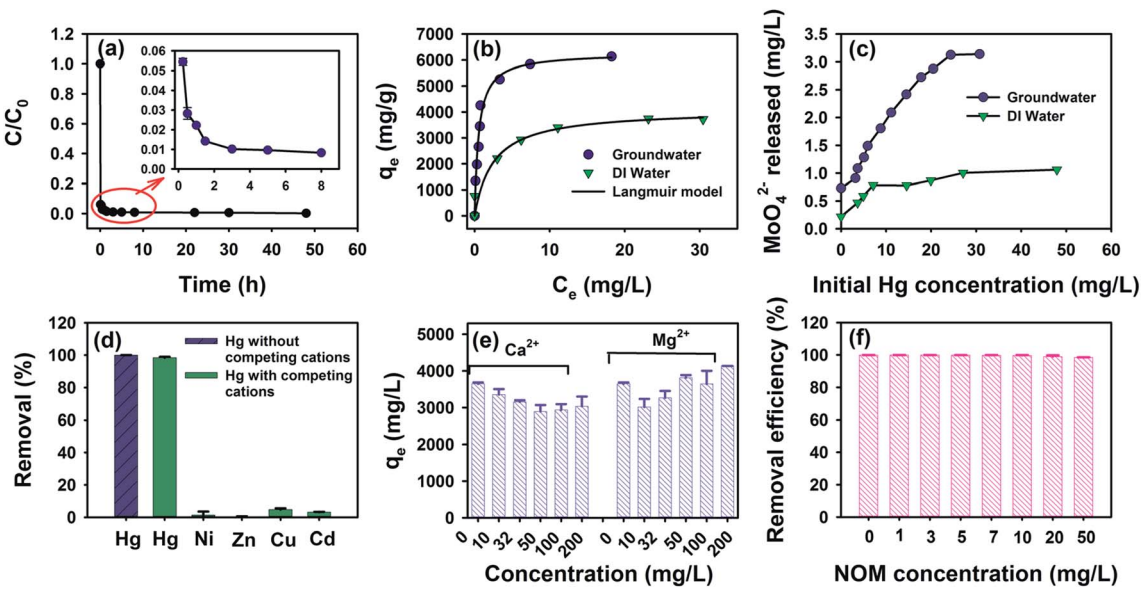

Fig. 2 Hg(II) removal by MoS_2 nanosheets. (a) Kinetics of Hg(II) uptake by MoS_2 nanosheets, $C_{Hg} = 5$ mg L^{-1} and $C_{MoS2} = 4$ mg L^{-1}; (b) isotherm of Hg(II) uptake by MoS_2 fitted with Langmuir model, $C_{Hg} = 0$–42 mg L^{-1}; (c) the concentration of MoO_4^{2-} in the solution after reaction between MoS_2 and Hg ions; (d) removal efficiency of various heavy metals by MoS_2 nanosheets in a mixture containing all cations at equal concentrations of 1 mg L^{-1}; (e) effects of Ca(II) and Mg(II) on Hg removal by MoS_2 nanosheets; (f) effects of NOM on Hg removal by MoS_2, $C_{Hg} = 20$ mg L^{-1} and $C_{MoS2} = 15$ mg L^{-1}.

at Hg removal reported previously including M-Ti_3C_2 nanosheets (~5.46 × 10^6 mL g^{-1}),[46] GO@SnS_2 (8.68 × 10^5 mL g^{-1}),[47] LHMS-1 (>1 × 10^6 mL g^{-1}),[48] and polymeric chelating fibers (3.0 × 10^5 to 3.8 × 10^6 mL g^{-1}).[49] The kinetic data were fitted with pseudo-first-order and pseudo-second-order models (Fig. S5†),[50] and fitting parameters and the results are summarized in Table S1.† As shown in Fig. S5b,† the pseudo-second-order kinetic model provided the better fitting with the higher R^2 (0.9999), which indicated that the rate-limiting step might be chemisorption between Hg and MoS_2 nanosheets.[51]

The removal isotherm in Fig. 2b shows that the Hg uptake density of MoS_2 nanosheets increased promptly at low equilibrium Hg concentrations and approached a constant value at high concentrations. The isotherm was better fitted with the Langmuir model (R^2 = 0.9801) than Freundlich model (R^2 = 0.9145, Table S2†), which suggested that removal of Hg was likely achieved *via* a monolayer coverage on homogeneous sites of the MoS_2 nanosheet surface.[52] According to the fitting, the maximum Hg uptake capacity by MoS_2 nanosheets in groundwater was determined to be 6288 mg g^{-1}, which is among the highest removal capacities for Hg reported to date and also higher than those of MoS_2 nanosheets synthesized by other methods (*i.e.*, 425–1991 mg g^{-1} in Table S3†). The superb remediation performance of MoS_2 nanosheets in our study stems from the good dispersity and monolayer structure, which give rise to maximum exposure of active sulfur sites for anchoring Hg ions. More interestingly, the removal capacity determined in this study also exceeds the theoretical Hg removal capacity by monolayer MoS_2 (*i.e.*, 2506 mg g^{-1}) if surface adsorption *via* Hg–S bonding is the sole removal mechanism.[31] Thus, other removal mechanisms (*e.g.*, reduction, electrostatic interactions, or complexation) might exist in the Hg removal by the MoS_2 nanosheets employed in this study. Considering the high redox potential of the Hg^{2+}/Hg^0 couple (E^0 = 0.85 V),[53] we measured the concentrations of the oxidation product of MoS_2, namely MoO_4^{2-}, after Hg removal to reveal if reductive removal of Hg occurred. The oxidation of MoS_2 to MoO_4^{2-} has been observed in previous studies and also validated experimentally in our own test (Fig. S6†).[37] As shown in Fig. 2c, the extent of oxidative dissolution of MoS_2 nanosheets was closely related to initial Hg concentrations. Specifically, if Hg was absent, the concentration of released MoO_4^{2-} was very low at 0.22 and 0.73 mg L^{-1} in DI water and groundwater, respectively, indicating that the extent of oxidation of MoS_2 by dissolved oxygen was insignificant; when the initial Hg addition was 25–30 mg L^{-1}, the concentration of released MoO_4^{2-} was ~3.1 mg L^{-1} amounting to ~80% of the total MoS_2 added, which indicates that Hg promoted the oxidation of MoS_2. The correlation of Hg removal and MoO_4^{2-} release indicates that a portion of Hg in the groundwater was likely removed *via* a redox reaction with MoS_2 nanosheets.

To evaluate the potential of using MoS_2 nanosheets in practical groundwater remediation, we also investigated the selectivity of MoS_2 nanosheets towards Hg cations in the presence of various ionic species found in groundwater. In the groundwater containing mixed heavy cations at the same concentration (Fig. 2d), MoS_2 nanosheets exhibited nearly complete removal of Hg(II) with an efficiency of 98.4%. In comparison, the removal efficiency was much lower (<5%) for other heavy metals such as Cu(II), Cd(II), Ni(II) and Zn(II). Additionally, the presence of concentrated competing Ca and Mg cations does not impact the Hg removal (Fig. 2e), because of the high affinity of MoS_2 to Hg ions and thus favorable removal of Hg over other competing cations. Meanwhile, Ca and Mg cations were not adsorbed noticeably by MoS_2 (Fig. S7†), in line with the low affinity of MoS_2 to hard Lewis acids. Moreover, the presence of NOM up to 50 mg L^{-1} has no influence on the Hg removal by MoS_2 (Fig. 2f), which is an advantage for MoS_2 compared to the inhibited Hg removal by NOM observed in other adsorbents previously (*e.g.*, FeS, oxide/Fe-Mn).[54,55]

It is interesting to note in Fig. 2b that a large Hg removal capacity by MoS_2 was observed in DI water (*i.e.*, 4043 mg g^{-1}), which is however slightly lower than that in groundwater (*i.e.*, 6288 mg g^{-1}). The oxidative dissolution of MoS_2 was apparently inhibited in DI water (Fig. 2c). Collectively, the decreased capacity and inhibited MoS_2 oxidation imply that the reduction-based Hg removal was weakened in DI water and also indicates that the groundwater matrix plays an important role in varying the efficiency and mechanism of Hg removal by MoS_2. Interestingly enough, the groundwater matrix has been reported to have negative impacts on the removal of heavy metals *via* competitive sorption of other cations and complexation of heavy metals with anions.[56,57] The contrary, enhanced Hg removal in groundwater by MoS_2 nanosheets is yet to be reported and is therefore investigated by using various characterization tools to assess the role of the matrix on the removal nature and extent.

3.3 Matrix-dependent Hg removal by MoS_2

To unravel the matrix-dependent Hg removal, the Hg-laden MoS_2 nanosheets were characterized by XRD, Raman, XPS and TEM after Hg removal in groundwater and DI water. As shown in Fig. 3a, Hg-laden MoS_2 formed in DI water exhibited no apparent peaks in the XRD spectra. In the groundwater matrix, however, the characteristic reflections of Hg_2Cl_2 (PDF #73-1247) were observed in the Hg-laden MoS_2. The formation of Hg_2Cl_2 in the groundwater was also confirmed with Raman spectra, in which the Raman band that is specific to Hg(I)–Hg(I) was observed at ~166 cm^{-1} (Fig. 3b).[58] Such a characteristic Raman peak for Hg(I) was absent for Hg-laden MoS_2 formed in DI water, and instead only MoS_2 peaks at 380 cm^{-1} and 405 cm^{-1} were observed. Both XRD and Raman spectra indicate that the reduction of Hg(II) by MoS_2 and precipitation of Hg(I) with the Cl ion (a major constituent in groundwater) were involved in the Hg removal from groundwater,[46] and Hg removal in DI water might occur by different Hg removal mechanisms.

XPS analysis was performed to characterize chemical compositions and oxidation states of Hg-laden MoS_2 formed in DI water and groundwater. The composition of Hg-laden MoS_2 shown in Fig. S8† confirmed the association of Cl with the Hg removal in the groundwater. Based on the deconvolution of Mo 3d XPS spectra (Fig. 3c), the Hg removal in DI water caused the partial oxidation of MoS_2 to Mo(V), which exhibits the

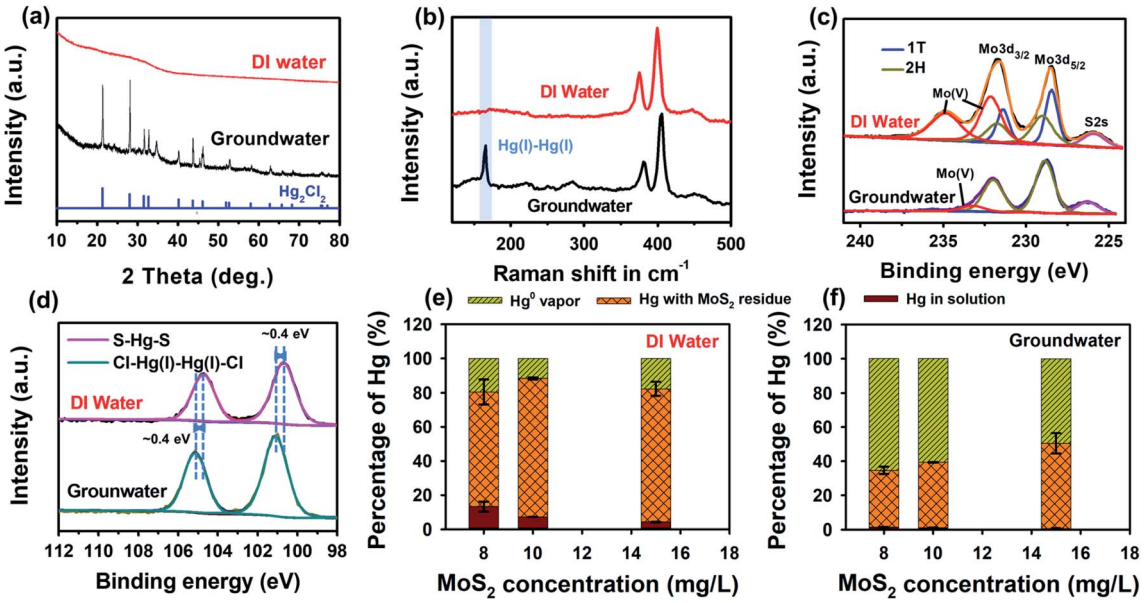

Fig. 3 Mechanistic investigation of Hg(II) removal by MoS_2 nanosheets in groundwater and DI matrices. (a) XRD patterns, (b) Raman spectra, (c) Mo 3d and (d) Hg 4f XPS spectra of Hg-laden MoS_2 formed in DI water and groundwater; Hg species distribution in the Hg-laden MoS_2 nanosheets formed in (e) DI water and (f) groundwater.

characteristic peaks of Mo $3d_{5/2}$ and Mo $3d_{3/2}$ at 232.1 and 234.8 eV, respectively. In groundwater, however, 1T-phase MoS_2 was completely degraded as shown in Fig. 3c, and 2H-phase MoS_2 became the main Mo residue after Hg remediation. The oxidation product of MoS_2 formed in groundwater could not be observed in the XPS spectra, because it existed as soluble MoO_4^{2-} species released into the groundwater solution (Fig. 2c). Hg 4f XPS spectra showed the Hg $4f_{7/2}$ and Hg $4f_{5/2}$ peaks of Hg_2Cl_2 formed in the groundwater were located at ~101.1 and 105.1 eV (Fig. 3d), respectively.[59] The appearance of Hg 4f peaks in Hg-laden MoS_2 formed in DI water was observed at even lower binding energy with a ~0.4 eV shift relative to those in groundwater, implying the complexation of Hg ions with multiple electron-donating S atoms on the MoS_2 surface. Actually, a downward shift of binding energy has been observed in the case of Pb(II) removal by MoS_2, in which Pb(II) binds to two neighboring S atoms with an equal bond length.[40] Hg(II) as a larger and softer Lewis acid is more likely to form a multi-bonding structure with S, in a similar manner to S–Hg–S arranged in a square planar configuration on the galena surface.[60] The TEM elemental mapping (Fig. S9†) of Hg-laden MoS_2 formed in groundwater exhibited similar element distribution patterns of Hg and Cl because of the formation of Hg_2Cl_2. Meanwhile, the overlap of Hg and S elements in the Hg-laden MoS_2 samples formed in DI water also confirms surface adsorption as one of the dominant removal mechanisms when chloride is absent (Fig. S10†).

It is worth noting that Hg^0, as the possible reduction product of Hg(II), was not observed in the XPS spectra of Hg-laden MoS_2. This might be due to the ultra-high vacuum conditions we employed in the XPS measurements, which could vaporize Hg^0. Thus we investigated the mass distribution of Hg species in different physical states to reveal the amount of Hg^0 generated during the Hg removal by MoS_2 nanosheets in the groundwater and DI water. After Hg removal in both water matrices, Hg species distribution—in solution, with the MoS_2 residue, and in the vapor phase—was calculated to represent the un-removed Hg, the Hg removed *via* surface adsorption or formation of Hg_2Cl_2, and reduction product Hg^0, respectively. The measurements of the mass content of Hg in each phase are described in the Methods, and the species distributions are shown in Fig. 3e and f for the removal in DI water and groundwater, respectively. In DI water, the adsorbed Hg was the major species amounting to ~70–80% of the total Hg (Fig. 3e), which confirmed that surface adsorption played the dominant role in the Hg removal by MoS_2 in the DI water. In the groundwater, the removed Hg predominantly existed as Hg^0 with percentages at 50–65% of the total Hg, and the remaining 35–50% of Hg species existed in the form of Hg_2Cl_2. Additionally, almost no residual Hg was detected in the groundwater as compared to ~10% residual Hg found in DI water, which is in line with the enhanced Hg removal performance associated with the groundwater matrix.

The Mo mass distribution results (Fig. S11†) revealed that the dissolved portion in the groundwater accounts for 57–82% of the total Mo added (8–15 mg L^{-1}), which is much larger than that in DI water (0.16–2.83%). The significantly enhanced oxidative dissolution of MoS_2 in the Hg-containing groundwater is in good agreement with the observation in Fig. 2c. Overall, the characterization and mass distribution of Hg-laden MoS_2 demonstrated that the groundwater matrix (*i.e.*, the presence of Cl) could promote the redox reactions between Hg and MoS_2, induce vast generation of reduced Hg species (*i.e.*, Hg^0 and monovalent Hg), and thus enhance the overall removal capacity of Hg by MoS_2 nanosheets as compared to the removal in DI water.

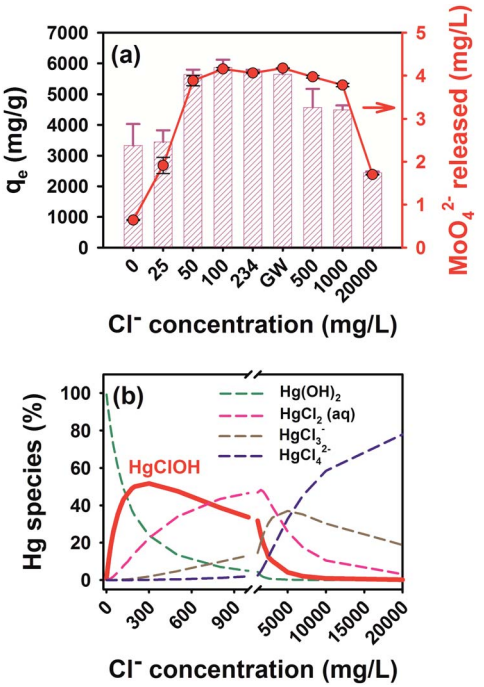

Fig. 4 Speciation-dependent Hg removal efficiency varied by Cl^- concentrations. (a) Effects of Cl^- on Hg removal by MoS_2, $C_{Hg} = 35$ mg $L^{-1}$and $C_{MoS_2} = 4$ mg L^{-1}. (b) Hg speciation as a function of Cl^- concentration determined by using Visual MINTEQ.

3.4 Cl^- effect on Hg removal efficiency and mechanisms

To reveal the role of chloride in the case of Hg removal by MoS_2, we measured the Hg removal capacities by MoS_2 in solutions containing various concentrations of Cl^-. As shown in Fig. 4a, the Hg uptake density of MoS_2 increased from ~3331 mg g^{-1} to ~5723 mg g^{-1} with increasing concentrations of Cl^- from 0 to ~234 mg L^{-1}, the typical Cl^- concentration in groundwater. Further increase of Cl^- to 500 mg L^{-1} and above would decrease the uptake density, eventually down to 2445 mg g^{-1} when the Cl^- concentration was 20 000 mg L^{-1}, typically found in seawater. The profile of MoS_2 oxidative release was in line with the Hg uptake trend, in which moderate Cl^- concentrations enhanced the release and the high Cl^- content inhibited the MoS_2 oxidative dissolution (Fig. 4a). The control test without Hg addition indicated that Cl^- alone did not change the MoS_2 oxidation and Mo release behavior (Fig. S12†).

To explain inverted U-shaped Hg removal as a function of Cl^- concentration, the distribution of soluble Hg species as a function of Cl^- concentration was calculated by using Visual Minteq (Fig. 4b).[55] At the concentration of Cl^- in the chosen groundwater, soluble Hg predominantly exists as HgClOH at ~51% (Fig. S13†). HgClOH species exhibit a similar inverted U-shaped pattern to the Hg removal in response to various Cl^- concentrations: the formation of HgClOH was promoted at moderate Cl^- concentrations (0 to 300 mg L^{-1}) but was inhibited at high Cl^- concentrations (800 mg L^{-1} above), where the dominant Hg species shifted to Cl^- complexed Hg such as $HgCl_2$, $HgCl_3^-$, and $HgCl_4^{2-}$ (Fig. 4b). The inhibition of these stable aqueous Hg(II) complexes in the Hg reductive and adsorptive removal has been observed previously.[55,61–63]

Considering the strong correlation between Hg removal capacity and HgClOH percentages, we proposed the following steps that may account for the enhanced Hg removal in groundwater. First, HgClOH was adsorbed onto the surface of MoS_2 *via* Hg–S bonding owing to the high affinity of S atoms as a soft Lewis base to Hg species, followed by the split of adsorbed HgClOH into $^{\bullet}OH$ and $^{\bullet}HgCl$ radicals on the MoS_2 surface.[46] The homolytic cleavage of the Hg–O bond has been found to be a spontaneous step with a small energy barrier if any to overcome in the previous study.[46] Consequently, $^{\bullet}HgCl$ radicals could either dimerize into the Hg_2Cl_2 precipitate ($K_{sp} = 5 \times 10^{-20}$)[64] or accept another electron from MoS_2 and reduce to Hg^0.[65] Owing to the stability of Hg(I) associated with Cl, the stepwise reduction of Hg(II) by MoS_2 was favored leading to the enhanced total Hg removal. Meanwhile the resulting $^{\bullet}OH$ radicals caused nearly complete oxidation of MoS_2 to soluble Mo and S species.[66] In DI water, however, the reductive removal of Hg is slow because uncomplexed Hg(I) is not stable and direct two-electron reduction is kinetically inhibited.[53] Thermodynamically, the formation of Hg_2^{2+} associated with Cl is also favored over direct reduction to Hg^0 because the redox potential E° for the Hg^{2+}/Hg_2^{2+} couple (0.91 V) is greater than that for the Hg^{2+}/Hg^0 couple (0.85 V).[53]

The importance of HgClOH in the reductive removal of Hg(II) by MoS_2 can also be demonstrated by the pH-varied Hg removal. Fig. S14† exhibits the declined Hg removal efficiency by MoS_2 nanosheets under lower pH conditions, which could be partially explained by the decreased amounts of HgClOH formed under these conditions. Specifically, the Hg removal efficiency decreased from 94.2% to 33.2% as the equilibrium pH was adjusted from 7.9 to 3.0. The Hg species distribution as a function of pH is shown in Fig. S14b,† which clearly shows the conversion of the dominant Hg species from HgClOH to $HgCl_2$ when the pH was lowered. The correlation of HgClOH dominance with the highest Hg removal efficiency at pH 8 supports the finding that the HgClOH species contribute to the reductive removal and thus enhance the overall removal efficiency. In addition, low pH conditions would decrease the Hg removal efficiency *via* the protonation and charge-neutralization of MoS_2 nanosheets.[55,67]

3.5 Toward practical application of MoS_2 in Hg remediation

For engineered remediation use, immobilization of Hg on materials is of great importance to minimize the migration, bioavailability and toxicity of Hg.[50] Activated carbon (AC), as a common adsorbent for heavy metal remediation in groundwater,[68] was chosen as a reference for comparison. The Hg removal capacity by AC was determined to be 55.5 mg g^{-1} (Fig. S15†), much lower than that of MoS_2. Consequently, significantly high dosage of AC (~200 times as much as MoS_2 used) has to be employed to achieve a similar Hg loading mass onto the remediation materials. The Hg release behavior of the Hg-laden MoS_2 nanosheets and AC was examined with fresh groundwater, acid solution (mass ratio of H_2SO_4 and HNO_3 at

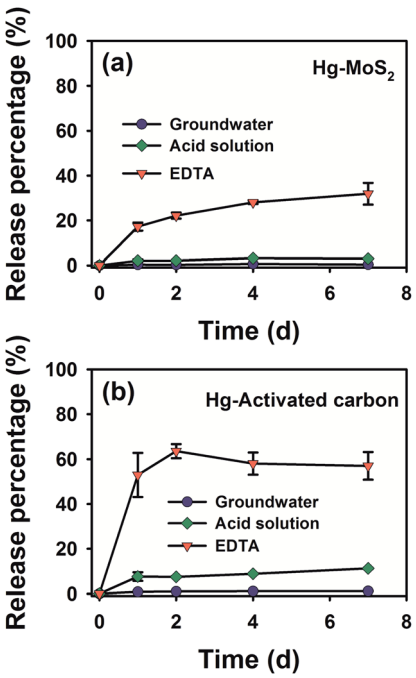

Fig. 5 Desorption kinetics of Hg from (a) MoS_2 and (b) activated carbon in the groundwater, acid solution, and EDTA solution, initial $C_{Hg} = 20$ mg L^{-1}, $C_{MoS_2} = 8$ mg L^{-1}, $C_{AC} = 1.67$ g L^{-1}.

2 : 1, pH = 3.20 ± 0.05), and EDTA solution, to simulate the natural state fluid, acid rain, and strong metal complexing agent, respectively.[69,70] Generally, as shown in Fig. 5a and b, the amount of released Hg from MoS_2 or AC increased slowly over 1 d, and then gradually reached an equilibrium in 2–4 d. Upon equilibrium, the desorption efficiencies of Hg-laden MoS_2 were 0.4%, 3.0%, and 28% (the ratio of desorbed Hg over the actual amount of Hg immobilized by MoS_2 estimated from Fig. 3f) in the simulated groundwater, acid solution, and EDTA solution, respectively, as compared to apparently higher desorption degrees of 1.2%, 12%, and 60% in the case of AC (Fig. 5b). These results indicated that MoS_2 has stronger Hg immobilization capability against release in various types of extractants, which is more conducive to the remediation of Hg pollution in the groundwater environment.

Despite the strong immobilization of Hg by MoS_2, the redox reactions between Hg(II) and MoS_2 nanosheets are potential concerns towards the practical applications of MoS_2 in the remediation of Hg-containing groundwater. Hg reduction could decrease the content of soluble Hg(II) that is readily available for conversion to more toxic MeHg by microbial activities. However, it may also unintendedly lead to the generation of toxic Hg^0 vapor.[71] Additionally, MoS_2 overdose and the oxidative release of MoO_4^{2-} may cause secondary pollution. To address these concerns, the concentration of MoS_2 should be optimized in practical applications, and the fate and transport behaviors of the remaining MoS_2 should be investigated to evaluate the environmental risks. Phase engineering of MoS_2 is also suggested for future studies to enhance the chemical stability of MoS_2 and to minimize the redox reactions between oxidants (*e.g.*, Hg(II) and dissolved oxygen) and 1T-MoS_2, and thus eliminate the release of potential hazardous secondary species.[35] Also, the *ex situ* treatment of Hg-containing groundwater with MoS_2 is suggested at the current stage to better manage the remediation process and avoid the uncontrollable release.

4. Conclusions

Our study demonstrated that the groundwater matrix has profound implications on the Hg removal efficiency and mechanisms by MoS_2 nanosheets. In DI water free of Cl^-, MoS_2 nanosheets remove Hg with a moderate capacity *via* adsorption as the dominant mechanism. In this mechanism, Hg ions are selectively removed over other divalent cations because of the strong affinity to MoS_2 *via* Lewis soft–soft interactions and are likely to complex with multiple S atoms on the MoS_2 surface. In groundwater containing Cl^-, the formation of HgClOH, as the major species, kinetically and thermodynamically promotes the reduction of Hg(II) to Hg_2Cl_2 and Hg^0, which becomes the predominant removal mechanism. This reduction-based removal further enhances the total Hg removal capacity of MoS_2 nanosheets to ~6288 mg g^{-1}, which is among the highest values reported for Hg to date. Considering the excellent dispersity of MoS_2, stability of Hg-laden MoS_2, and low toxicity of MoS_2,[72] we believe that MoS_2 nanosheets have great potential in the remediation of Hg-contaminated groundwater. Additionally, our work suggests that future studies should consider matrix effects on the performance of remediation materials in the groundwater environment.

Author contributions

Mengxia Wang: methodology, investigation, data analysis, visualization, writing – original draft; Qi Han: investigation, data analysis; Yufei Shu: investigation, data analysis; Kunkun Wang: investigation, data analysis; Li Wang: investigation, data analysis; Bei Liu: investigation, data analysis, writing – review & editing; Ines Zucker: writing – review & editing; Zhongying Wang: supervision, project administration, writing – review & editing.

Conflicts of interest

There is no conflict of interest for this research.

Acknowledgements

This work was financially supported by the National Nature Science Foundation of China (No. 22076075 and 41907296). The authors acknowledge the assistance of SUSTech Core Research Facilities.

References

1 I. Ghodbane and O. Hamdaoui, Removal of mercury(II) from aqueous media using eucalyptus bark: kinetic and equilibrium studies, *J. Hazard. Mater.*, 2008, **160**, 301–309.

2 A. Radwan, I. M. El-Sewify, A. Shahat, H. M. E. Azzazy, M. M. H. Khalil and M. F. El-Shahat, Multiuse Al-MOF Chemosensors for Visual Detection and Removal of Mercury Ions in Water and Skin-Whitening Cosmetics, *ACS Sustainable Chem. Eng.*, 2020, **8**, 15097–15107.
3 Z. Tang, F. Fan, S. Deng and D. Wang, Mercury in rice paddy fields and how does some agricultural activities affect the translocation and transformation of mercury - A critical review, *Ecotoxicol. Environ. Saf.*, 2020, **202**, 110950.
4 L. Zhang and M. H. Wong, Environmental mercury contamination in China: sources and impacts, *Environ. Int.*, 2007, **33**, 108–121.
5 P. Li, X. B. Feng, G. L. Qiu, L. H. Shang and Z. G. Li, Mercury pollution in Asia: A review of the contaminated sites, *J. Hazard. Mater.*, 2009, **168**, 591–601.
6 H. Cheng and Y. Hu, Mercury in Municipal Solid Waste in China and Its Control: A Review, *Environ. Sci. Technol.*, 2011, **46**, 593–605.
7 A. Bollen, A. Wenke and H. Biester, Mercury speciation analyses in $HgCl_2$-contaminated soils and groundwater-implications for risk assessment and remediation strategies, *Water Res.*, 2008, **42**, 91–100.
8 M. A. Hashim, S. Mukhopadhyay, J. N. Sahu and B. Sengupta, Remediation technologies for heavy metal contaminated groundwater, *J. Environ. Manage.*, 2011, **92**, 2355–2388.
9 Y. Huang, S. Xia, J. Lyu and J. Tang, Highly efficient removal of aqueous Hg^{2+} and CH_3Hg^+ by selective modification of biochar with 3-mercaptopropyltrimethoxysilane, *Chem. Eng. J.*, 2019, **360**, 1646–1655.
10 S.-I. Lo, P.-C. Chen, C.-C. Huang and H.-T. Chang, Gold Nanoparticle–Aluminum Oxide Adsorbent for Efficient Removal of Mercury Species from Natural Waters, *Environ. Sci. Technol.*, 2012, **46**, 2724–2730.
11 X. Lu, X. Huangfu, X. Zhang, Y. Wang and J. Ma, Strong enhancement of trace mercury removal from aqueous solution with sodium thiosulfate by *in situ* formed Mn-(hydr)oxides, *Water Res.*, 2014, **65**, 22–31.
12 M. M. Matlock, B. S. Howerton and D. A. Atwood, Irreversible precipitation of mercury and lead, *J. Hazard. Mater.*, 2001, **84**, 73–82.
13 L. Y. Blue, P. Jana and D. A. Atwood, Aqueous mercury precipitation with the synthetic dithiolate, $BDTH_2$, *Fuel*, 2010, **89**, 1326–1330.
14 S. Chiarle, M. Ratto and M. Rovatti, Mercury removal from water by ion exchange resins adsorption, *Water Res.*, 2000, **34**, 2971–2978.
15 Y. K. Henneberry, T. E. C. Kraus, J. A. Fleck, D. P. Krabbenhoft, P. M. Bachand and W. R. Horwath, Removal of inorganic mercury and methylmercury from surface waters following coagulation of dissolved organic matter with metal-based salts, *Sci. Total Environ.*, 2011, **409**, 631–637.
16 M. S. Islam, R. J. Vogler, S. M. Abdullah Al Hasnine, S. Hernández, N. Malekzadeh, T. P. Hoelen, E. S. Hatakeyama and D. Bhattacharyya, Mercury Removal from Wastewater Using Cysteamine Functionalized Membranes, *ACS Omega*, 2020, **5**, 22255–22267.
17 J. G. Yu, B. Y. Yue, X. W. Wu, Q. Liu, F. P. Jiao, X. Y. Jiang and X. Q. Chen, Removal of mercury by adsorption: a review, *Environ. Sci. Pollut. Res.*, 2016, **23**, 5056–5076.
18 M. De, R. Azargohar, A. K. Dalai and S. R. Shewchuk, Mercury removal by bio-char based modified activated carbons, *Fuel*, 2013, **103**, 570–578.
19 S. Kabiri, D. N. H. Tran, S. Azari and D. Losic, Graphene-Diatom Silica Aerogels for Efficient Removal of Mercury Ions from Water, *ACS Appl. Mater. Interfaces*, 2015, **7**, 11815–11823.
20 C. G. Weisener, K. Scott Sale, a. D. A. Smyth and D. W. Blowes, Field Column Study Using Zerovalent Iron for Mercury Removal from Contaminated Groundwater, *Environ. Sci. Technol.*, 2005, **39**, 6306–6312.
21 D. S. Han, M. Orillano, A. Khodary, Y. Duan, B. Batchelor and A. Abdel-Wahab, Reactive iron sulfide (FeS)-supported ultrafiltration for removal of mercury (Hg(II)) from water, *Water Res.*, 2014, **53**, 310–321.
22 G. R. Bhagure and S. R. Mirgane, Heavy metal concentrations in groundwaters and soils of Thane Region of Maharashtra, India, *Environ. Monit. Assess.*, 2011, **173**, 643–652.
23 J. Liu, Y. Peng, C. Li, Z. Gao and S. Chen, An investigation into the hydrochemistry, quality and risk to human health of groundwater in the central region of Shandong Province, North China, *J. Cleaner Prod.*, 2021, **282**, 125416.
24 Y. Sun, Y. Liu, Z. Lou, K. Yang, D. Lv, J. Zhou, S. A. Baig and X. Xu, Enhanced performance for Hg(II) removal using biomaterial (CMC/gelatin/starch) stabilized FeS nanoparticles: stabilization effects and removal mechanism, *Chem. Eng. J.*, 2018, **344**, 616–624.
25 Q. Zeng, L. Hu, H. Zhong, Z. He, W. Sun and D. Xiong, Efficient removal of Hg^{2+} from aqueous solution by a novel composite of nano humboldtine decorated almandine (NHDA): Ion exchange, reducing-oxidation and adsorption, *J. Hazard. Mater.*, 2021, **404**, 124035.
26 W. Li, M. C. Tekell, Y. Huang, K. Bertelsmann, M. Lau and D. Fan, Synergistic High-Rate Solar Steaming and Mercury Removal with MoS_2/C @ Polyurethane Composite Sponges, *Adv. Energy Mater.*, 2018, **8**, 1802108.
27 Z. Li, R. Fan, Z. Hu, W. Li, H. Zhou, S. Kang, Y. Zhang, H. Zhang and G. Wang, Ethanol introduced synthesis of ultrastable 1T-MoS_2 for removal of Cr(VI), *J. Hazard. Mater.*, 2020, **394**, 122525.
28 Z. Wang, A. Sim, J. J. Urban and B. Mi, Removal and Recovery of Heavy Metal Ions by Two-dimensional MoS_2 nanosheets performance and mechanisms, *Environ. Sci. Technol.*, 2018, **52**, 9741–9748.
29 Z. Wang, Q. Tu, A. Sim, J. Yu, Y. Duan, S. Poon, B. Liu, Q. Han, J. J. Urban, D. Sedlak and B. Mi, Superselective Removal of Lead from Water by Two-Dimensional MoS_2 Nanosheets and Layer-Stacked Membranes, *Environ. Sci. Technol.*, 2020, **54**, 12602–12611.
30 Z. Wang and B. Mi, Environmental Applications of 2D Molybdenum Disulfide (MoS_2) Nanosheets, *Environ. Sci. Technol.*, 2017, **51**, 8229–8244.

31 K. Ai, C. Ruan, M. Shen and L. Lu, MoS_2 Nanosheets with Widened Interlayer Spacing for High-Efficiency Removal of Mercury in Aquatic Systems, *Adv. Funct. Mater.*, 2016, **26**, 5542–5549.

32 C. Liu, S. Zeng, B. Yang, F. Jia and S. Song, Simultaneous removal of Hg^{2+}, Pb^{2+} and Cd^{2+} from aqueous solutions on multifunctional MoS_2, *J. Mol. Liq.*, 2019, **296**, 111987.

33 F. Jia, Q. Wang, J. Wu, Y. Li and S. Song, Two-Dimensional Molybdenum Disulfide as a Superb Adsorbent for Removing Hg^{2+} from Water, *ACS Sustainable Chem. Eng.*, 2017, **5**, 7410–7419.

34 C.-B. Ma, Y. Du, B. Du, H. Wang and E. Wang, Investigation of an eco-friendly aerogel as a substrate for the immobilization of MoS_2 nanoflowers for removal of mercury species from aqueous solutions, *J. Colloid Interface Sci.*, 2018, **525**, 251–259.

35 Z. Wang, A. v. d. Bussche, Y. Qiu, T. M. Valentin, K. Gion, A. B. Kane and R. H. Hurt, Chemical Dissolution Pathways of MoS_2 Nanosheets in Biological and Environmental Media, *Environ. Sci. Technol.*, 2016, **50**, 7208–7217.

36 W. Zou, Q. Zhou, X. Zhang and X. Hu, Dissolved Oxygen and Visible Light Irradiation Drive the Structural Alterations and Phytotoxicity Mitigation of Single-Layer Molybdenum Disulfide, *Environ. Sci. Technol.*, 2019, **53**, 7759–7769.

37 C. L. Fausey, I. Zucker, D. E. Lee, E. Shaulsky, J. B. Zimmerman and M. Elimelech, Tunable Molybdenum Disulfide-Enabled Fiber Mats for High-Efficiency Removal of Mercury from Water, *ACS Appl. Mater. Interfaces*, 2020, **12**, 18446–18456.

38 W. Zhan, F. Jia, Y. Yuan, C. Liu, K. Sun, B. Yang and S. Song, Controllable incorporation of oxygen in MoS_2 for efficient adsorption of Hg^{2+} in aqueous solutions, *J. Hazard. Mater.*, 2020, **384**, 121382.

39 F. Jia, X. Zhang and S. Song, AFM study on the adsorption of Hg^{2+} on natural molybdenum disulfide in aqueous solutions, *Phys. Chem. Chem. Phys.*, 2017, **19**, 3837–3844.

40 Z. Wang, Q. Tu, A. Sim, J. Yu, Y. Duan, S. Poon, B. Liu, Q. Han, J. J. Urban, D. L. Sedlak and a. B. Mi, Superselective Removal of Lead from Water by Two Dimensional MoS_2 Nanosheets and Layer-stacked Membranes, *Environ. Sci. Technol.*, 2020, **54**, 12601–12611.

41 H. Dong and I. M. C. Lo, Transport of Surface-Modified Nano Zero-Valent Iron (SM-NZVI) in Saturated Porous Media: Effects of Surface Stabilizer Type, Subsurface Geochemistry, and Contaminant Loading, *Water, Air, Soil Pollut.*, 2014, **225**, 2107.

42 Q. Yan, C. Lian, K. Huang, L. Liang, H. Yu, P. Yin, J. Zhang and M. Xing, Constructing an Acidic Microenvironment by MoS_2 in Heterogeneous Fenton Reaction for Pollutant Control, *Angew. Chem.*, 2021, **60**, 17292–17300.

43 W. Ding, L. Hu, J. Dai, X. Tang, R. Wei, Z. Sheng, C. Liang, D. Shao, W. Song, Q. Liu, M. Chen, X. Zhu, S. Chou, X. Zhu, Q. Chen, Y. Sun and S. X. Dou, Highly Ambient-Stable 1T-MoS_2 and 1T-WS_2 by Hydrothermal Synthesis under High Magnetic Fields, *ACS Nano*, 2019, **13**, 1694–1702.

44 E. Er, H.-L. Hou, A. Criado, J. Langer, M. Möller, N. Erk, L. M. Liz-Marzán and M. Prato, High-Yield Preparation of Exfoliated 1T-MoS_2 with SERS Activity, *Chem. Mater.*, 2019, **31**, 5725–5734.

45 S. Shi, Z. Sun and Y. H. Hu, Synthesis, stabilization and applications of 2-dimensional 1T metallic MoS_2, *J. Mater. Chem. A.*, 2018, **6**, 23932–23977.

46 K. Fu, X. Liu, D. Yu, J. Luo, Z. Wang and J. C. Crittenden, Highly Efficient and Selective Hg(II) Removal from Water Using Multilayered $Ti_3C_2O_x$ MXene *via* Adsorption Coupled with Catalytic Reduction Mechanism, *Environ. Sci. Technol.*, 2020, **54**, 16212–16220.

47 E. Rathore and K. Biswas, Selective and ppb level removal of Hg(II) from water: synergistic role of graphene oxide and SnS_2, *J. Mater. Chem. A.*, 2018, **6**, 13142–13152.

48 M. J. Manos, V. G. Petkov and M. G. Kanatzidis, $H_{2x}Mn_xSn_{3-x}S_6$ ($x = 0.11$–0.25): A Novel Reusable Sorbent for Highly Specific Mercury Capture Under Extreme pH Conditions, *Adv. Funct. Mater.*, 2009, **19**, 1087–1092.

49 C. Liu, Y. Huang, N. Naismith and J. Economy, Novel Polymeric Chelating Fibers for Selective Removal of Mercury and Cesium from Water, *Environ. Sci. Technol.*, 2003, **37**, 4261–4268.

50 M. Wang, Y. Li, D. Zhao, L. Zhuang, G. Yang and Y. Gong, Immobilization of mercury by iron sulfide nanoparticles alters mercury speciation and microbial methylation in contaminated groundwater, *Chem. Eng. J.*, 2020, **381**, 122664.

51 F. Jia, C. Liu, B. Yang, X. Zhang, H. Yi, J. Ni and S. Song, Thermal Modification of the Molybdenum Disulfide Surface for Tremendous Improvement of Hg^{2+} Adsorption from Aqueous Solution, *ACS Sustainable Chem. Eng.*, 2018, **6**, 9065–9073.

52 G. Tan, W. Sun, Y. Xu, H. Wang and N. Xu, Sorption of mercury (II) and atrazine by biochar, modified biochars and biochar based activated carbon in aqueous solution, *Bioresour. Technol.*, 2016, **211**, 727–735.

53 A. Amirbahman, D. B. Kent, G. P. Curtis and M. C. Marvin-DiPasquale, Kinetics of Homogeneous and Surface-Catalyzed Mercury(II) Reduction by Iron(II), *Environ. Sci. Technol.*, 2013, **47**, 7204–7213.

54 Y. Huang, Y. Gong, J. Tang and S. Xia, Effective removal of inorganic mercury and methylmercury from aqueous solution using novel thiol-functionalized graphene oxide/Fe–Mn composite, *J. Hazard. Mater.*, 2019, **366**, 130–139.

55 Y. Gong, Y. Liu, Z. Xiong and D. Zhao, Immobilization of mercury by carboxymethyl cellulose stabilized iron sulfide nanoparticles: reaction mechanisms and effects of stabilizer and water chemistry, *Environ. Sci. Technol.*, 2014, **48**, 3986–3994.

56 J. P. H. Perez, A. A. Schiefler, S. N. Rubio, M. Reischer, N. D. Overheu, L. G. Benning and D. J. Tobler, Arsenic removal from natural groundwater using 'green rust': Solid phase stability and contaminant fate, *J. Hazard. Mater.*, 2021, **401**, 123327.

57 G. Qu, L. Kou, T. Wang, D. Liang and S. Hu, Evaluation of activated carbon fiber supported nanoscale zero-valent iron for chromium (VI) removal from groundwater in a permeable reactive column, *J. Environ. Manage.*, 2017, **201**, 378–387.

58 M. Crippa, S. Legnaioli, C. Kimbriel and P. Ricciardi, New evidence for the intentional use of calomel as a white pigment, *J. Raman Spectrosc.*, 2021, **52**, 15–22.
59 N. D. Hutson, B. C. Attwood and K. G. Schecke, XAS and XPS Characterization of Mercury Binding on Brominated Activated Carbon, *Environ. Sci. Technol.*, 2007, **41**, 1747–1752.
60 J. Bower, K. S. Savage, B. Weinman, M. O. Barnett, W. P. Hamilton and W. F. Harper, Immobilization of mercury by pyrite (FeS_2), *Environ. Pollut.*, 2008, **156**, 504–514.
61 T. S. Pasakarnis, M. I. Boyanov, K. M. Kemner, B. Mishra, E. J. O'Loughlin, G. Parkin and M. M. Scherer, Influence of Chloride and Fe(II) Content on the Reduction of Hg(II) by Magnetite, *Environ. Sci. Technol.*, 2013, **47**, 6987–6994.
62 M. M. Hyland, G. E. Jean and G. M. Bancroft, XPS and AES studies of Hg(II) sorption and desorption reactions on sulphide minerals, *Geochim. Cosmochim. Acta*, 1990, **54**, 1957–1967.
63 Y. Sun, Z. Lou, J. Yu, X. Zhou, D. Lv, J. Zhou, S. A. Baig and X. Xu, Immobilization of mercury (II) from aqueous solution using Al_2O_3-supported nanoscale FeS, *Chem. Eng. J.*, 2017, **323**, 483–491.
64 L. Fan, A. Zhou, L. Zhong and Y. Liu, Photoinduced reduction of high concentration Hg(II) to Hg_2Cl_2 from acid wastewater with the presence of fulvic acid under anaerobic conditions, *Chemosphere*, 2018, **198**, 13–20.
65 Y. Wang, G. Liu, Y. Li, Y. Liu, Y. Guo, J. Shi, L. Hu, Y. Cai, Y. Yin and G. Jiang, Occurrence of Mercurous [Hg(I)] Species in Environmental Solid Matrices as Probed by Mild 2-Mercaptoethanol Extraction and HPLC-ICP-MS Analysis, *Environ. Sci. Technol. Lett.*, 2020, **7**, 482–488.
66 J. Ji, Q. Yan, P. Yin, S. Mine, M. Matsuoka and M. Xing, Defects on CoS_{2-x}: Tuning Redox Reactions for Sustainable Degradation of Organic Pollutants, *Angew. Chem.*, 2021, **133**, 2939–2944.
67 D. Xu, X. L. Tan, C. L. Chen and X. K. Wang, Adsorption of Pb(II) from aqueous solution to MX-80 bentonite: Effect of pH, ionic strength, foreign ions and temperature, *Appl. Clay Sci.*, 2008, **41**, 37–46.
68 D. Huang, G. Wang, Z. Shi, Z. Li, F. Kang and F. Liu, Removal of hexavalent chromium in natural groundwater using activated carbon and cast iron combined system, *J. Cleaner Prod.*, 2017, **165**, 667–676.
69 S. Debnath, D. Nandi and U. C. Ghosh, Adsorption–Desorption Behavior of Cadmium(II) and Copper(II) on the Surface of Nanoparticle Agglomerates of Hydrous Titanium(IV) Oxide, *J. Chem. Eng. Data*, 2011, **56**, 3021–3028.
70 Y. Huang, M. Wang, Z. Li, Y. Gong and E. Y. Zeng, *In situ* remediation of mercury-contaminated soil using thiol-functionalized graphene oxide/Fe-Mn composite, *J. Hazard. Mater.*, 2019, **373**, 783–790.
71 K. Kritee, J. D. Blum, M. W. Johnson, B. A. Bergquist and T. Barkay, Mercury Stable Isotope Fractionation during Reduction of Hg(II) to Hg(0) by Mercury Resistant Microorganisms, *Environ. Sci. Technol.*, 2007, **41**, 1889–1895.
72 Z. Wang, A. V. D. Bussche, Y. Qiu, T. M. Valentin, K. Gion, A. B. Kane and a. R. H. Hurt, Chemical Dissolution Pathways of MoS_2 Nanosheets in Biological and Environmental Media, *Environ. Sci. Technol.*, 2016, **50**, 7208–7217.